eprints@whiterose.ac.uk
https://eprints.whiterose.ac.uk/

Automated Decision Support System for Lung Cancer Detection and Classification via Enhanced RFCN with Multilayer Fusion RPN

Anum Masood, Bin Sheng, *Member, IEEE*, Po Yang, *Senior, IEEE*, Ping Li, *Member, IEEE*, and David Dagan Feng, *Fellow, IEEE*

Abstract—Detection of lung cancer at early stages is critical, radiologists read computed tomography (CT) images to prescribe follow-up treatment. The conventional method for detecting nodule presence in CT images is tedious. We propose an enhanced multidimensional Region-based Fully Convolutional Network (mRFCN) based automated decision support system for lung nodule detection and classification. The mRFCN is used as an image classifier backbone for feature extraction along with the novel multi-Layer fusion Region Proposal Network (mLRPN) with position-sensitive score maps (PSSM) being explored. We applied a median intensity projection to leverage three-dimensional information from CT scans and introduced deconvolutional layer to adopt proposed mLRPN in our architecture to automatically select potential region-of-interest. Our system has been trained and evaluated using LIDC dataset, and the experimental results showed the promising detection performance in comparison to the state-of-the-art nodule detection/classification methods, achieving a sensitivity of 98.1% and classification accuracy of 97.91%.

Index Terms—Lung cancer, nodule classification, convolutional neural network, computer aided systems.

I. INTRODUCTION

LUNG cancer is considered to be a major cause of death worldwide. Almost 1.6 million people die in a year due to pulmonary cancer. In 2018, pulmonary cancer has caused 142,670 deaths alone in the US [1]. Pulmonary cancer is a disease indicated by the uncontrollable growth of abnormal pulmonary cells. Most effective method for lung nodule detection in early stages is computed tomography scan owing to its ability to generate high resolution 3D chest images. Detection of lung cancer in the initial stages is crucial to patient's survival but it is tedious and difficult task since the radiologists manually marked nodule position and possibly miss lung nodules which have overlapping anatomical structures.

In the past decade, the lung cancer death rate is comparatively reduced owing to the advancements in the industrial

applications used for lung cancer detection and diagnosis. Different commercially available computer-aided systems have potential to tremendously increase the detection as well as the diagnosis accuracy even with high dimensional lung cancer dataset without annotation features for classification. CAD system for nodule detection comprises of Computer Aided Detection (CADe) and Computer Aided Diagnosis (CADx). The CADe aims to distinguish between the nodule candidates as non-nodule (anatomical structures like tissues, blood vessels) while CADx characterize these detected lesions and classifies them as benign or malignant tumors. The aim of these CAD systems primarily is to overall enhance the accuracy of cancer diagnosis by the radiologists while reducing the CT images interpretation time duration. In this way, these tools have become crucial to assist in their decision making.

With the introduction of deep learning techniques [2] particularly in object detection and feature extraction from big data, various computer-aided (CAD) systems based on deep learning are developed for real-world clinical use. These methods have significantly enhanced the quality and the efficiency of the healthcare sector particularly the screening process for lung cancer early detection. Although the innovations in pulmonary cancer are slow and unsteady in terms of survival rate as compared to the other cancer types yet deep learning methods have promising results and the detection systems based on deep learning techniques have declined the lung cancer death rate by the factor of 22% in the last 5 years. In this paper, we have proposed a novel CAD system for pulmonary nodule detection and classification. The key contributions of this paper are listed as follows.

- A novel deep convolutional neural network based model is proposed for early detection of lung cancer which is capable of using 3D spatial as well as contextual information yielding larger amount of discriminating feature map for nodule candidates detection.
- Novel multi-Layer fusion Region Proposal Network (mLRPN) is proposed for selection of potential region-of-interest (RoI) with position sensitive score maps (PSSM) to achieve high accuracy in nodule classification. We applied novel median intensity projection (MIP) to leverage three dimensional information from CT images, and integrated deconvolutional layer to adopt mLRPN for automatic RoI selection.
- The performance of proposed CAD system is validated

in two modes: mRFCN stand-alone and mRFCN Cloud based. Testing of both modes is done on LIDC dataset and clinical dataset from Shanghai Sixth People's Hospital (SPH). Furthermore, experimental results for the performance of the proposed method on the LIDC dataset show high precision and reduced false positive rate to a significant extent in comparison to the state-of-the-art nodule detection and classification methods.

II. RELATED WORK

In general, any CADe system for lung cancer comprise of four phases; pre-processing, lung segmentation, analysis of feature set and candidate nodule detection on the other hand CAD systems have two stages; nodule candidate detection and false positive (FP) reduction (see Fig. 1). For nodule detection, traditionally lung segmentation is done using 2D geometrical level set active contour, morphological features, 2D parametric deformable model, voxel clustering and multi gray-level thresholding. The limitation of these models was their dependency on the image and inability to detect nodules overlapping anatomic structures [3]. Several researchers have proposed various CADe systems to detect the lung nodules. Armato III et al. [4] proposed a CADe system which uses Linear Discriminant Analysis (LDA) method on 187 nodules (juxtaplueral and solitary nodules) resulting in sensitivity of approximately 70% while having 9.6 FP per case. Suzuki et al. [5] used the dataset of 121 nodules (juxtapleural, juxtavascular, solitary and ground-glass shaped lesions) while [6] developed MTANN (Massive Training Artificial Neural Network) for nodule detection. The initial nodule candidates are processed using filtering method in order to remove the false positive results. Supervised approaches are also developed to reduce the FP but these methods have high computational cost. Hierarchical VQ, LDA, ANN, SVM are few supervised reduction methods which are used for FP reduction [7]–[10]. In recent years deep learning is introduced in medical imaging, according to Setio et al. [11], there are numerous CAD systems using deep learning for nodule detection. Convolutional Neural Network (CNN) [12], Fully Convolutional Networks (FCN) [13], Multi-crop Convolutional Neural Network (MC-CNN) [14], and DFCNet [15] are CAD systems based on deep neural networks which are capable of classifying the detected nodules as benign or malignant tumors.

III. METHODS

A. Datasets

In the real application of Computer Aided Diagnosis (CAD) system, the screening stage is very crucial. Since it is a huge computation cost for using 3D CT scans volume, an alternation of using source pictures in axis direction is applicable. Therefore, we combined three neighboring CT scans for each axis direction, respectively. The potential candidates choice of search space can be further analyzed by selecting training sets of original CT scans.

B. Augmentation

In situations, where a limited amount of labeled data is available, neural networks tend to over-fit training dataset, because these models have large quantities of parameters. An efficient way to tackle this problem is data augmentation. Although part of the resultant samples from data augmentation might be similar to each other. During the data augmentation phase, each RoI goes through a series of image transformations for label-preserving, producing a huge amount of correlated newly acquired training data samples. Affine transformation namely translation, scaling and rotation are used. Mostly the training data samples obtained from data augmentation have a correlation, thus this step is recommended for data over-fitting reduction. We opted to augment malignant samples by cropping, duplicating, flipping, scaling and rotating copies in training dataset. Specifically, among input batch, random rotation were performed for up-sampling and down-sampling. We resampled training and testing cases to 3 mm since having common thickness method helped in attaining the homogeneity among all cases (training and testing) which further improved the dataset processing.

C. Architecture

1) Multiview Combination: Unlike traditional image classification problem where input channels are the same as the color channels of the image, CT scan generates gray-scale images. Another notion is that CT scans sets are originally 3D in which z axis to discriminate different positions of lung nodule, whereas the input image sets are 2D patches. Inspired by Hessian, we explore Median Intensity Projection (MIP) [16] to combine information from three dimensions of CT scans. We defined θ as image projected by MIP. With input image patch I, θ for three dimensions can be presented as:

$$\theta(q,r) = \underset{p}{med}\, I(p,q,r)$$
$$\theta(p,r) = \underset{q}{med}\, I(p,q,r) \qquad (1)$$
$$\theta(p,q) = \underset{r}{med}\, I(p,q,r)$$

where med denotes median operator. Different views can provide different information, while patches in combination with different dimensions can provide the space distribution of tumor tissues. In order to construct input image sets with three channels, we connected three MIP projected images together: $\theta = [\theta(q,r), \theta(p,r), \theta(p,q)]$.

The proposed multi-layer fusion region proposed network (mLRPN) is designed to improve the original RPN from Faster R-CNN [17] is designed to overcome the limitation of the previous related work targeted for object detection i.e. Faster R-CNN. Although the proposed work is inspired from the resnet of Faster R-CNN yet it has replaced 2D with 3D convolution layers. CT images can be processed by proposed MIP method to interactively viewing volumes of CT data, in which the CT number of each pixel is given by the minimum number of CT through the volume. Furthermore unlike the Faster R-CNN, the proposed mRFCN uses mLRPN which improves the RoI selection thus improving the performance of detection by the proposed method. Additional Deconvolutional
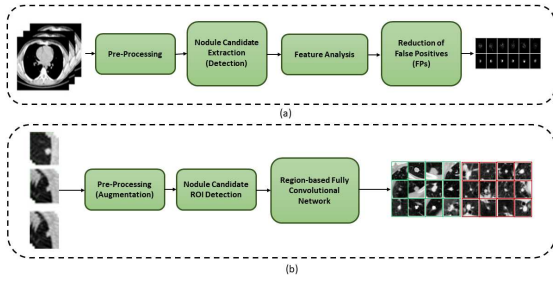
Fig. 1: (a) Basic Stages of Computer Aided Detection (CADe) System for Lung Nodules. (b) Stages of our proposed Computer Aided Detection System.

Fig. 2: Overview of the mRFCN architecture.

Fig. 3: Our proposed anchor in multi-Layer fusion Region Proposal Network (mLRPN).

layer improved the original RPN from Faster R-CNN. The deconvolutional layer upsampled the features learned from the input. Traditionally, Faster R-CNN depends on the skip connection linked with the deconvolution layer on the upsampling for generating initial results but the deconvolution layer is unable to recover the small-sized objects such as nodules which are lost after the downsampling. Therefore, they cannot accurately detect small-sized nodules. In our proposed method, we used deconvolutional layer which ensured the recovery of any loss of small objects such as lung nodules in the downsampling process. The challenge for Faster R-CNN in case of lung nodule detection is that it cannot detect the diverse sized objects using limited labeled dataset. To mitigate this we proposed novel method, mLRPN has improved feature extraction (multi-resolution) and we used multiple layers for region proposal generation i.e. multi-angle, multi-size and multi-shape. For efficient selection of the ROI, we proposed to merge all the RoI which were extracted from multi-layers in a single layer as shown in overview of the mRFCN in Fig. 2.

2) Multi-Layer Region Proposal Network (mLRPN): A prevalent method for selecting region of interest (RoI) is to split original CT scans into small sample windows: 8×8, 16×16, and 32×32. For our proposed work, we selected the mini-window, whose spatial window contains the central of malignant nodule according to the marked-up annotation from experienced thoracic radiologists, as positive training or testing samples. Such a strategy has an obvious disadvantage that if a specific nodule is larger than pre-fixed sample window or some nodule is located across two sample windows, then it will be discarded. This disadvantage will lead to inaccurate construction of training or testing sets, and further lead to low classification performance. In order to address the problems mentioned above and select several RoI efficiently, we proposed a novel multi-Layer fusion Region Proposal Network (mLRPN). In the mLRPN, in order to improve the ability to detect nodules of different scales, shape and orientation, we designed a three layer multi-RPN; multi-size v_{L1}^u, multi-angle θ_{L1}^g, and multi-shape d_{L3}^j which generate rectangular object proposals set using the image (irrespective of size) as its input, and further calculates objectness value for each set [17]. We observed that malignant nodule occupy relatively small proportion of CT scans compared to conventional object
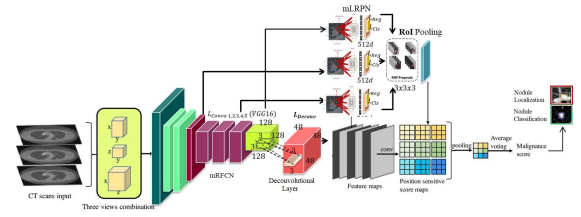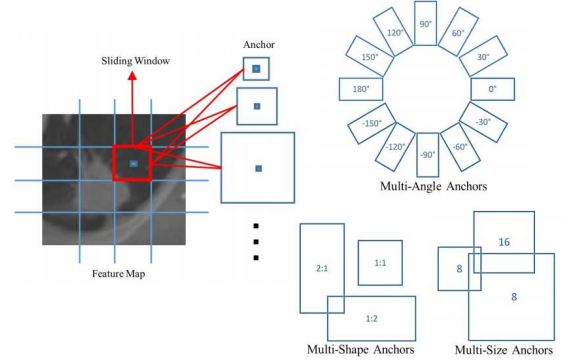
recognition tasks where object takes up a larger space in the image. Since VGG-16 Net contains several max pooling layers, which inevitably reduce the image size [18], resulting in the relatively small nodule distorted. Gaining inspirations from previous success of Long [19], we proposed a deconvolutional layer, 4 kernel size and 4 stride size, to be added after the last feature extracting layer. This deconvolutional layer is aimed to recover the original CT scans size by upsampling (see Fig. 2 for our proposed system).

According to [20], we use a tiny network N to slide through the activation (feature) map output M_{out} by the final added deconvolutional layer. We also defined this tiny network N to take 3×3 spatial windows of the input activation(feature) map M_{in} with each spatial window w being mapped to 512 dimension feature. The feature will be fed into box-classification layer (cls) and regression layer (reg), respectively. As for the choice for anchor [21] size shown in Fig. 3, we explore large quantities of nodule boundary size, and generate six different sizes v_{L1}^u (u represents anchor size) of reference boxes centered at each sliding window location for our multi-size layer. In order to contain nodules of different malignant level, we choose anchor sizes of 4×4, 8×8, 12×12, 20×20, 26×26, 32×32, respectively (see Fig. 3). As the nodule spreads in all direction therefore, we proposed multi-angle layer, in which we rotated RPN with 12 different angles θ_{L2}^g where g represents angle i.e. 0,30,60,90,120,150,180,-150,-120,-90,-60, and -30 degrees rotation from center of sliding window. Lastly, we proposed multi-shape layer d_{L3}^j where j shows different shapes based on the anchor's width to height ratio;1:1, 2:1 and 1:2.

3) Multidimensional Region-based Fully Convolutional Network (mRFCN): With mLRPN proposing RoI, we apply
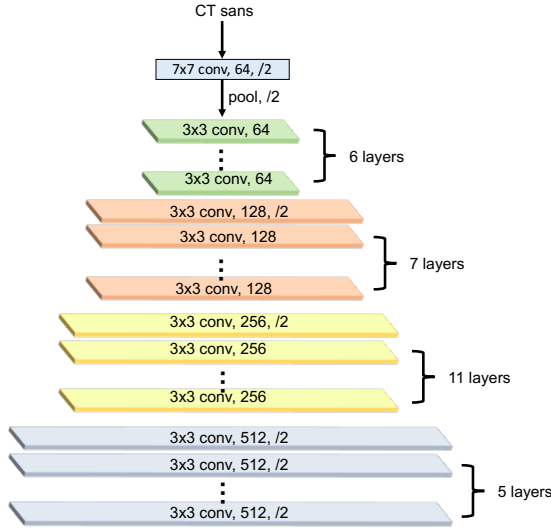
Fig. 4: Detailed configuration of our proposed multidimensional Region-based Fully Convolutional Network (mRFCN).

Region-based Fully Convolutional Network [22] to predict presence of nodule or the malignancy level if nodule exists. Our architecture is inspired from ResNet-101 [23] which is based on the VGG nets, comprising of 3×3 filters with the convolutional network. In ResNet-101, if the filters and layers are comparable then the feature map size remains the same but in order to maintain time complexity for each layer when activation map size is halved, the number of the filters should be doubled. In mRFCN, we excluded the fully convolutional layer and the mean pooling layer for efficient computation of the feature maps. In case of similar dimensions for both the output and input, the identity alternatives can be directly used:

$$q = \mathbb{F}(p, \{W_i\}) + p \qquad (2)$$

where p and q denotes input and output vectors, respectively, that are fed into and considered by each network layer. The function $\mathbb{F}(p, \{W_i\})$ shows the residual mapping which is to be learn. There are two alternate solutions in case the input dimensions increase. If no extra parameters are already present then the identify mapping's dimensions are increased by zero entries padding. Another way is to add 1×1 convolutional layer to match dimension with shortcut projection. The stride for both options is 2. Unlike ResNet-101, our proposed model uses convolutional layer solely to compute the feature map, therefore, the learnable weights are computed using convolutional layers and shared on the whole image. The architecture design of mRFCN is shown in Fig. 4.

Using the radiologist annotations, we add a $k \times k (5 + 1)$-channel convolutional layer (4×4) as the output layer to generate position sensitive score maps (PSSM). Where 4 represents five malignant level of lung nodule, 1 represents non-nodule, and we divide mLRPN proposed RoI into 4×4 grid cell. Specifically, for 32×32 proposed rectangular, each divided grid has the size of 8×8. Therefore, $4 \times 4 \times 6$ score maps were generated, and we used the average pooling

operation to calculate the relevance score to 6 categories for each split bin:

$$\zeta_c(w, h \mid \phi) = \sum_{(a,b) \in bin(w,h)} z_{w,h,c}(a + a_0, b + b_0 \mid \phi)/n \quad (3)$$

where ϕ denotes parameters of the network, $\zeta_c(w, h \mid \phi)$ is the relevance score of (w, h)th bin to malignant category c, $z_{w,h,c}$ is the score map generated by last convolutional layer, (a_0, b_0) is the top-left corner of RoI, and n denotes the total pixel number in the bin. With $4 \times 4 \times 6$ relevance scores ζ being calculated, we decide the malignancy level of the RoI by average voting and also apply cross-entropy evaluation for ranking of RoI:

$$\zeta_c(\phi) = \sum_{w,h} \zeta_c(w, h \mid \phi) \qquad (4)$$

$$\xi_c(\phi) = \exp(\zeta_c(\phi)) / \sum_{\iota=0}^{5} \exp(\zeta_\iota(\phi)) \qquad (5)$$

Here $\zeta_c(\phi)$ denotes the relevance score for RoI to class c, and $\xi_c(\phi)$ is the softmax response for class c.

Following [21], [23] we also applied bounding box regression to generate 4-dimension bounding box vector $t = (t_x, t_y, t_w, t_h)$, the parameters are defined as:

$$
\begin{aligned}
t_x &= (x - x_a)/w_a \\
t_y &= (y - y_a)/h_a \\
t_w &= \log(w/w_a) \\
t_h &= \log(h/h_a)
\end{aligned} \qquad (6)
$$

where (x, y) denotes the box's central position, and w represents the width and h shows the box height. The variables above with subscript a are the corresponding parameters for anchor box (see Fig. 3). We add a sliding $4 \times 4 \times 4$ -d convolutional layer for bounding box regression. After we obtained $4 \times 4 \times 4$ score maps bank, we simply use position-sensitive region of interest pooling on them, further we get $4 \times 4 \times 4$ dimensional vector for each region of interest. The position-sensitive RoI pooling layer is used to leverage position sensitive score in each grid. The whole computation process is almost cost-free since there is no supervised learning layer following the RoI layer.

D. Loss Function

In the training process, with RPN to provide region proposal, we define our loss function by merging box regression as well as the cross-entropy loss:

$$\{L\}_{t,\xi} = -\log(\xi_{c^*}) + \{\frac{1}{N_r}\} \sum \{L\}_r(t, t^*) \qquad (7)$$

$$\{L\}_r(t, t^*) = \begin{cases} 0.5(t - t^*)^2, & \{if \ |t - t^*| < 1\} \\ |t - t^*| - 0.5, & \{otherwise\} \end{cases} \qquad (8)$$

where the left part of equation 7 denotes classification cross entropy loss [23], N_r is the input number of Regression layer, $\mathbb{L}_r$ is similar to the bounding box regression loss as presented in [17], and t^* denotes ground truth values. Positive samples

---

Algorithm 1 Multidimensional Region-based Fully Convolutional Network Training Procedure

---

1: **procedure** MULTIDIMENSIONAL REGION-BASED FULLY CONVOLUTIONAL NETWORK TRAINING PROCEDURE($B, b, n, S, \alpha, \beta_1, \beta_2$)
2:     **Inputs:**
3:     B: RoI sample batch size;
4:     b: mini-batch size;
5:     S: Rescale image size;
6:     α: Adam stepsize;
7:     n: Training iteration;
8:     $\beta_1, \beta_2 \in [0, 1)$: Exponential decay rate for moment estimates;
9:     **Initialization:**
10:     Initialize $\tilde{w}^0 = 0$ (Initialize network parameter vector);
11:     **Pre-process dataset:**
12:     Construct 3-dim dataset using Median Intensity Projection according to Eq. (1);
13:     Rescale dataset into S;
14:     **for** $s = 0, 1, 2, ..., n$ **do**
15:         **Forward Pass:**
16:         Generate feature map with multidimensional-RFCN architecture;
17:         Generate M Region of Interest;
18:         **for** $m = 0, 1, 2, ..., M$ **do**
19:             Construct loss function for RoI_m using Eq. (6);
20:         **end for**
21:         **Backpropagation:**
22:         RoIs sorting by loss (positive RoIs and negative RoIs);
23:         Selection of highest loss $\mathbb{L}$ in set B RoIs;
24:         Gradient estimation $g_s = \frac{\sum_{i \in B} \nabla \mathbb{L}_i}{B}$;
25:         $m_{s+1} = \beta_1 \cdot m_s + (1 - \beta_1) \cdot g_s$ (Updating of biased 1st moment estimate)   ▷ Adam process;
26:         $v_{s+1} = \beta_2 \cdot v_s + (1 - \beta_2) \cdot g_s^2$ (Updating of biased 2nd raw moment estimate);
27:         $\hat{m}_{s+1} = m_{s+1}/(1 - \beta_1^{s+1})$ (Computation of bias-corrected 1st moment estimate);
28:         $\hat{v}_{s+1} = v_{s+1}/(1 - \beta_2^{s+1})$ (Compute bias-corrected 2nd raw moment estimate);
29:         $\tilde{w}^{s+1} = \tilde{w}^s - \alpha \cdot \hat{m}_{s+1}/(\sqrt{\hat{v}_{s+1}} + \epsilon)$;
30:     **end for**
31:     **return** $\tilde{w}^n$ (the tuned network parameter);
32: **end procedure**

---

are represented by RoIs which have an intersection-over-union (IoU) protrude with ground-truth box of minimum 0.5, and alternatively, negative. In our mRFCN training procedure, the computation cost of RoI is negligible which enables the example mining to be cost free. We first construct the 3D dataset using MIP and then re-scale the dataset as pre-defined size. We followed the standard procedure to iteratively tune our network parameters. In the forward pass, the input CT scans are generated with higher dimensional feature map and M RoIs are generated using RPN, we then follow the loss function to evaluate M proposals loss. After sorting RoIs (both the positives RoIs and negatives RoIs) by loss, the highest loss of B RoIs is selected. In order to leverage the gradient information from selected batches, we perform average gradient operation on the B samples and use it as the input gradient estimation for Adam process to iteratively optimize our designed neural network. The detailed training procedure is summarized in Algorithm 1.

E. Implementation Details

We initialized the network using LIDC pre-trained basic model and the weights of layers in our proposed model. In the first step we freeze all layers in basic model with only training the layers of mRFCN and multi-layer fusion RPN (mLRPN). Secondly, the whole network is trained within two stages by decreasing learning rate. Following the common used settings in Faster R-CNN, the input images are firstly normalized and then we employed mRFCN architecture. The experiment was conducted on Ubuntu 16.04.3 LTS with 4 processors, Intel(R) Xeon(R) CPU E5-2686 v4 @ 2.3GHz and 64GB total memory space. Our model is trained on Tesla K80 with 12GB Memory. As for Region-based Fully Convolutional Network, we choose to use Intel Extended Caffe since the convolution layer, max pooling layer and fully connection layer in caffe is self-adaptive to the shape of input. Some other common libraries used include numpy 1.13.1, SimpleITK 1.1.0, pandas 0.19.2, sklearn 0.18.2. The training process of mRFCNN is done in 3 hours on Nvidia Tesla K80 graphic card. Training process used standard back-propagation using stochastic gradient descent (weight decay: 0.00045, momentum:0.12 and learning rate of 0.02 with increasing factor of 15 after five hundred iterations).

F. Cloud-Based Multidimensional Region-Based FCN

For clinical validation of mRFCN, we collaborated with the Shanghai Sixth People's Hospital. As a stand-alone CAD system, our proposed method performed well but to further improve the performance of our proposed method, we integrated cloud computing (Infrastructure as a Service (IaaS) by providing Virtual Machines, and Software as a Service (SaaS) by giving our mRFCN model) into our CAD system as shown in Fig. 5. In Cloud-Based mRFCN, we have four modules; data submission, online medical reports submission by radiologists of SPH, CAD result access, and physicians feedback, Firstly, the medical systems from SPH sent CT images of patients to the cloud storage using the router gateway. To record the physiological information of patients, we used body area network (BAN) comprising of multiple sensors attached to patients body. Furthermore, gateways are used to forward this acquired physiological data to cloud storage for processing. Afterward, our proposed mRFCN model is used to screen the CT images for nodules. Cloud storage enabled the storage of a vast amount of clinical data on which the proposed method was trained, the CT-images are processed by the mRFCN resulting in the marked nodules and their classification as malignant or benign. These results are considered as second opinion by the radiologists for making final diagnosis decision. The diagnosis decision is sent for real-time analysis by the physicians who
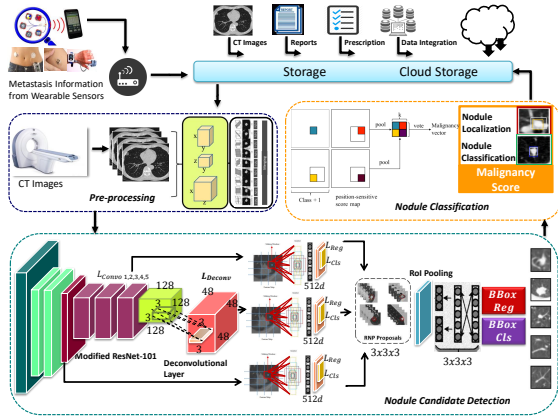
Fig. 5: Pipeline for our proposed decision support system. Firstly, we used body area network (BAN) and CT-scan to collect comprehensive physiological information and CT images of patient which were forwarded to cloud storage. Secondly, we applied affine transformations on CT-images for data-augmentation. Furthermore, we pre-processed CT images using multi-view combination. We used mRFCN model on these pre-processed CT images for nodule candidate detection. Meanwhile, multi-layer fusion region proposal networks (mL-RPN) with three layer of designed multi-anchors are applied to obtain the RoI proposals. Finally, we utilize position-sensitive score maps (PSSM) to classify detected nodules into two classes i.e. Benign and Malignant. The marked location of the nodule and the classification results are stored on the cloud for the physicist's reference for diagnosis and treatment.

determine the disease level and send the regular check-up notifications, reports, as well as treatment prescription to the patient. The regular check-up reports, disease status and the response of patient to the treatment is stored on the cloud storage for further data analysis and improvement of our proposed CAD system. Currently, we are able to deploy 10 VMs, and 24 processing units (cores) in our dedicated cloud back-end. For each case the complete processing time is 11-12 minutes. Open-source tool, HTCondor, was used for real-time optimization and monitoring of computing resources, thus the users have updated responsive CAD system.

IV. RESULTS AND DISCUSSIONS

Every year, around 1.59 million deaths are caused by Lung Nodule. It is essential to use CAD system to help radiologists to detect and diagnose pulmonary cancer. For developing a reliable CAD system, it should provide high performance in terms of diagnosis speed, quantity, accurate evaluation and overall low error rate. In state-of-art, the prevalent criteria for CAD system performance are two kinds of rate: sensitivity and false positive. The performance of proposed CAD system is validated in two modes: mRFCN stand-alone and mRFCN Cloud based. Testing of both modes is done on LIDC dataset and clinical dataset. Furthermore, the Nodule detection results of proposed CAD system are compared with state-of-the-art CAD systems using Free-Response Receiver Operating Characteristic (FROC) curve including average sensitivity and

TABLE I: Lung nodule features from radiologist.

Features	Descriptions
Internal structure	Soft tissue, fluid
Calcification	Popcorn, solid
Margin	Poorly defined, intermediate
Lobulation	Marked, intermediate
Spiculation	Marked, intermediate
Sphericity	Linear, ovoid
Texture	Non-solid, Part solid/(mixed)

TABLE II: Classifiers' Accuracy, Sensitivity and FPs/Scan Comparison to detect lung cancer based on Leave-One-Out Validation Method.

Classifiers	Accuracy (%)	Sensitivity (%)	FPs/Scan
CNN [12]	80.8	79.6	3.63
MTANNs [6]	88.6	86.53	2.62
FCN [13]	91.2	91.14	3.16
MC-CNN [14]	87.14	77.3	2.97
mRFCN	92.1	94.4	2.21
mRFCN (Using mLRPN)	97.91	98.1	2.19

number of false positives per scan (FPs/scan) as evaluation metric, where detection is considered a true positive if the location lies within the radius of a nodule centre while the Nodule Classification performance analysis, is done using area under the ROC curve (AUROC) which shows the performance of our proposed method on candidates' classification as nodules or non-nodules. In CAD system, when predicting the existence of nodule, we make comparison with the ground truth annotation, the false positive ratio is the probability of falsely rejecting the null hypothesis for particular test.

We calculate FP with ratio between the number of non-nodule samples are mistakenly predict as lung nodule with certain level of malignancy and the total amount of non-nodule samples. We give the definition of FP rate as:

$$\frac{FP}{N} = \frac{FP}{FP + TN} \tag{9}$$

$$SP = \frac{TP}{TP + FN} \tag{10}$$

SP, FP, FN, and TP denotes sensitivity, false positive, false negative and true positive rate, respectively. In our experiment, if a sample with nodule is not predicted as disease in our CAD system, it is FN. If a sample with nodule is predicted correctly, it represents TP. The performance evaluation of our proposed CAD system is done on the subset of LIDC-IDRI [24]. We consider the 1000 CT subsets, from LIDC-IDRI-0001 to LIDC-IDRI-1000. Note originally LIDC-IDRI contains 1018 CT scans sets in total. Every CT scan has around 300 slices, and each slice of which is gray level picture in size of 512*512, the slice thickness is 3 mm. We reconstruct all the images using sharp kernel (Siemens B50 kernel). For testing the performance accuracy of our CAD system for detecting pulmonary nodules, we excluded the CT scans which are inconsistent in slice spacing or have missing slice. After that procedure, we finally make a list of 892 CT

TABLE III: Performance Comparison of Proposed CADe with state-of-the-art CAD systems to detect lung cancer based on Leave-One-Out Validation Method.

CAD systems	Sensitivity (%)	FPs/Scan
Suzuki et al. [5]	80.3	4.8
Ye et al. [7]	90.2	8.2
Messay et al. [8]	80.4	3.0
Cascio et al. [9]	87	6.1
Han et al. [10]	82.7	4.0
mRFCN	94.4	2.21
mRFCN with mLRPN	98.1	2.19

scans. We significantly reduced the quantity of the non-nodule data samples since they are the majority component of CT scans, which impact the accuracy of CAD system with large quantity of presence. We give the definition of distinct features in appearance of nodule in Table I.

We use Leave-one-out Validation method to validate our CAD classifier's generalization performance. We randomly divided the CT scans from our dataset into training sets and testing sets, training sets are used to train our CAD classifiers and testing sets are used to validate the performance of CAD classifiers. The effectiveness of mRFCN is verified by comparing with existing methods CNN [12], MTANNs [6], FCN [13], and MC-CNN [14], the results are depicted in Table II. From Table II, we can deduce that mRFCN's performance is highest achieving a sensitivity of 92.1% and 94.4% accuracy with a lowest FP rate of 2.21 per CT Scan among state-of-art CAD system. The results indicate the superiority of mRFCN as CAD system for nodule detection. The comparison between 'mRFCN' and 'mRFCN (Using mLRPN)' indicates the proposed CAD system with three layer multi-anchor (multi-size, multi-angle, multi-shape) parameter setting performs better for RPN in candidate selection both in terms of sensitivity and accuracy which are recorded to be 98.1% and 97.91%, respectively.

Although different CAD systems are experimented on variable data sets which makes the relative comparison a difficult task, we still made the comparison between our proposed system with previous published CAD systems to investigate the perspectives of our mRFCN system since the average FPs/Scan is comparable and the comparison results are shown in Table III. In the experiment with nodule detection, data analysis is different from binary classification problem that each image might contain multiple lung nodule and more than one FPs/scan. Therefore, the conventional ROC curve is not suitable to analyze the performance of our CAD system. In order to handle this problem, we apply Free-response ROC (FROC) analysis [25]. A prevalent method [11] for evaluating mRFCN curve is used. The sensitivity of FROC curve is a function plotted on the mean number of FPs/scan. The mean FROC-score is calculated as the sensitivity mean at 7 FPs: 8, 4, 2, 1, 1/2, 1/4, and 1/8 FPs/scan. Table IV and Table V show the quantitative results of our proposed approach in comparison with others.

Fig. 6 shows the different CAD systems for nodule detection
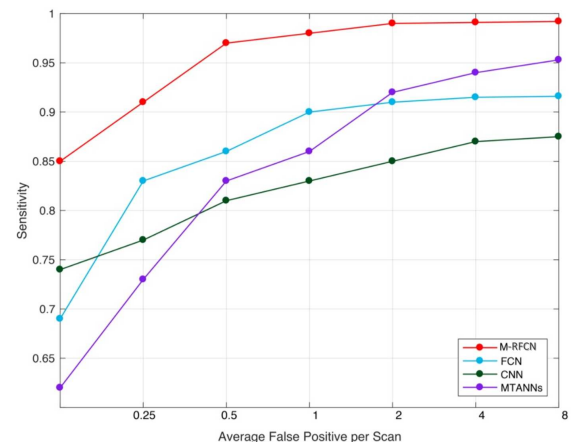

Fig. 6: FROC curve comparison between our proposed mR-FCN system and other existing CAD system.
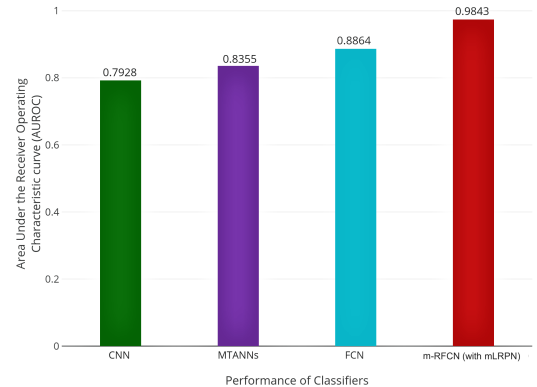

Fig. 7: AUROC based performance analysis of existing methods versus our proposed CADe system.

in terms of FROC curves, it is evident that our proposed mR-FCN system has achieved the most satisfactory performance amongst other tested CAD systems. It should be considered that mRFCN (red line) keeps high sensitivity even in the region where FPs per Scan is low. Although MTANNs have a high sensitivity value of over 89% when FPs per Scan reaches 4, but the sensitivity value of MTANNs drop significantly as FPs per Scan become small, which is impractical in real world clinical environment. A summary of our proposed CAD system and other CAD systems comparison in terms of AUROC is depicted in Table VI

Fig. 8 shows true nodules (marked in green) that were missed in the traditional CNN method, but is detected by our proposed method, when the false positives per scan lies within the range 1 to 4 with the sensitivity of 0.9813. The false negatives are marked in red which have similar appearance to nodules but our proposed system detected them as non-nodules using the characteristics of lung nodules obtained by our mRFCN, such as the example in Fig. 8 third row marked in red. We obtained few false negatives results as the data was not enough to represent that kind of nodules in training phase of our region-based FCN. In Table VI, we can see area under the FROC curve of the proposed system reaches highest

TABLE IV: Quantitative measurements of Sensitivity, mean FROC-score, FP Rate (FPs/scan), Specificity, Mean Accuracy, Inference Time for our proposed method in comparison with DFCNet in different mode (Stand-alone or Cloud Based).

CAD System	Dataset	System Mode	Sensitivity	mean FROC-score	FPs/scan	Specificity	Mean Accuracy	Inference Time
mRFCN (Using mLRPN)	LIDC-IDRI	Stand-Alone	98.1	44.6	2.19	93.2	97.91	∼180s
		Cloud-Based	95.2	48.3	2.1	94.5	96.7	∼150s
	Clinical Dataset	Stand-Alone	96.2	51.5	2.2	88.1	94.3	∼175ms
		Cloud-Based	97.6	52.2	2.4	91.4	95.5	∼120ms
mRFCN	LIDC-IDRI	Stand-Alone	94.4	41.6	2.21	89.2	92.1	∼180s
		Cloud-Based	95.2	42.3	2.1	90.3	90.7	∼150s
	Clinical Dataset	Stand-Alone	92.2	52.7	2.9	86.1	91.3	∼175ms
		Cloud-Based	90.3	54.1	2.4	87.4	89.5	∼120ms
DFCNet [15]	LIDC-IDRI	Stand-Alone	89.32	29.3	2.9	83.91	86.02	∼80s
		Cloud-Based	91.4	39.1	3.2	79.1	88.4	∼90s
	Clinical Dataset	Stand-Alone	96.17	53.5	1.17	83.67	86.32	∼190ms
		Cloud-Based	93.2	55.0	1.4	80.1	88.6	∼150ms

TABLE V: Quantitative results associated with training and testing errors for LIDC-IDRI and clinical datasets.

Dataset	mRFCN	Training Error	Testing Error
LIDC-IDRI [24]	Stand-Alone CAD	0.00418	0.00361
	Cloud-Based CAD	0.00471	0.00298
Clinical Dataset	Stand-Alone CAD	0.00364	0.00288
	Cloud-Based CAD	0.00394	0.00224

TABLE VI: AUROC-based performance comparison of existing methods versus our proposed CAD system.

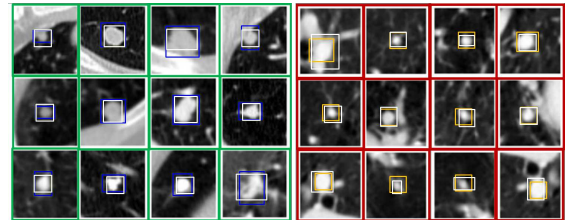| Classifiers	AUROC	Classes
CNN [12]	0.7928	Malignant
MTANNs [6]	0.8355	Malignant & Benign
FCN [13]	0.8864	Malignant & Benign
MC-CNN [14]	0.9330	Malignant & Benign
mRFCN	0.9813	Malignant & Benign

Fig. 8: Nodules detected as True Positives Malignant (green outline) and True Positives Benign (red outline) from the proposed CADe system. White boxes mark the ground truth and results produced by our CADe systems are marked by blue or yellow boxes. Blues boxes and yellow boxes are respectively denoting the malignant and benign nodules on the basis of malignancy score at 98.1% sensitivity.

value i.e. 0.9813, we are confident that our proposed system is the most suitable to use in clinics to detect and diagnose of pulmonary nodule, since the most CAD system will be applied in clinical environment to detect nodule where the false positives per scan is setting from 1 to 4 mostly. The experimental results presented in Fig. 7 demonstrate the superiority in generalization of our proposed mRFCN CAD system. To quantitatively evaluate the results for our proposed method, we have measured Standard Deviation Error Rate (Std $e_{D,C}$), Mean ANODE (mAN) Score and Processing-time (Time) of the CT images in the testing set of our clinical dataset with LDA [4], Rule Based Scheme [26], Cascade Classifier [27], Fuzzy Matching [28], Fisher Linear Discriminant (FLD) [29], SVM [30], Feature Pyramid Network (FPN) [31], Sequential Forward Selection (SFS) [32], Cluster Based Classifier [33], 3DDCNN [34] techniques. It can be seen in Table VII that, our proposed method achieved comparatively good results for Standard Deviation Error Rate, classification sensitivity (Sensitivity), FPs per case and computational duration (of around 219 ± 25.47 seconds) over other methods.

Qualitative results from the performance comparison between our mRFCN based CAD system versus state-of-the-art

Fig. 9: Malignant Nodules (red boxes) and Benign Nodules (blue boxes) from the mRFCN based CADe system. Green boxes mark the ground truth and compared to the results produced by our CADe systems are marked by red or blue boxes. Classification is based on the malignancy score at 98.1% sensitivity.

CAD system on having a confidence threshold of 95%. Green represents the Ground truth box. Red boxes are predicted as malignant nodules by our mRFCN method while blue represents benign nodules predictions. Four random cases out

of 120 cases from Shanghai Sixth's Hospital are selected. In Fig.9, left-most images (a) show the ground truth of lung CT scan, images (b) on in all cases show the predictions of malignant as well as benign nodules prediction of our proposed mRFCN model with confidence scores as high as 92.5%.

Table VII describes scoring criteria that are: statistical parameters such as mean ANODE Score, Standard Deviation which is used for both types of error rates i.e. Detection error rate and Classification error rate. Std $e_{D,C}$ indicate deviation from perfect detection, the metric Stde_D represents the standard deviation error rate between the radiologists from Shanghai Sixth People's Hospital nodule detection and the detection done by mRFCN and the term Stde_C represents the nodule classification by doctors from Shanghai Sixth People's Hospital and mRFCN classification. Computed results are presented in Table VII.

V. CONCLUSION

The solid criteria for a well performing CAD system is to help the expert radiologist in the process of lung cancer detection as providing them with helpful reference opinion. In this article, we have proposed a novel CAD system using multidimensional region-based fully convolutional networks, where we applied median intensity projection to extract useful information from the nodule dataset combining three dimension view, we proposed multi-layer fusion region proposed network (mLRPN) in our architecture by using deconvolutional layer to improve the original RPN from Faster R-CNN. Our CAD system not only indicates presence of nodule, but also gives the location as well as outlines the possible shape of the detected nodule along with classification of the detected nodule as benign or malignant. Our proposed system has been trained and evaluated using LIDC dataset and clinical dataset, the results from our experiments demonstrate that our proposed system has attained the sensitivity of 98.1% and classification accuracy of 97.91 %. In future, we aim to focus on the detection of some micro nodules where the diameter is less than 3 mm such that our CAD system works well with all kinds of nodules while maintaining its performance in sensitivity and FP/Scan.

REFERENCES

[1] R. L. Siegel, K. D. Miller, and A. Jemal, "Cancer statistics, 2019," *CA: A Cancer Journal for Clinicians*, vol. 69, no. 1, pp. 7–34, 2019.

[2] H. Gao, M. Yi, J. Yu, J. Li, and X. Yu, "Character segmentation-based coarse-fine approach for automobile dashboard detection," *IEEE Transactions on Industrial Informatics*, vol. 15, no. 10, pp. 5413–5424, 2019.

[3] R. K. Samala, H.-P. Chan, C. Richter, L. Hadjiiski, C. Zhou, and J. Wei, "Analysis of deep convolutional features for detection of lung nodules in computed tomography," in *Medical Imaging 2019: Computer-Aided Diagnosis*, vol. 10950, p. 109500Q, International Society for Optics and Photonics, 2019.

[4] S. G. Armato III, M. L. Giger, C. J. Moran, J. T. Blackburn, K. Doi, and H. MacMahon, "Computerized detection of pulmonary nodules on CT scans," *RadioGraphics*, vol. 19, no. 5, pp. 1303–1311, 1999.

[5] K. Suzuki, S. G. Armato III, F. Li, S. Sone, and K. Doi, "Massive training artificial neural network (MTANN) for reduction of false positives in computerized detection of lung nodules in low-dose computed tomography," *Medical Physics*, vol. 30, no. 7, pp. 1602–1617, 2003.

[6] D. Kumar, A. Wong, and D. A. Clausi, "Lung nodule classification using deep features in CT images," in *Conference on Computer and Robot Vision*, pp. 133–138, 2015.

[7] X. Ye, X. Lin, J. Dehmeshki, G. Slabaugh, and G. Beddoe, "Shape-based computer-aided detection of lung nodules in thoracic CT images," *IEEE Transactions on Biomedical Engineering*, vol. 56, no. 7, pp. 1810–1820, 2009.

[8] T. Messay, R. C. Hardie, and S. K. Rogers, "A new computationally efficient CAD system for pulmonary nodule detection in CT imagery," *Medical Image Analysis*, vol. 14, no. 3, pp. 390–406, 2010.

[9] D. Cascio, R. Magro, F. Fauci, M. Iacomi, and G. Raso, "Automatic detection of lung nodules in CT datasets based on stable 3D mass–spring models," *Computers in Biology and Medicine*, vol. 42, no. 11, pp. 1098–1109, 2012.

[10] H. Han, L. Li, F. Han, B. Song, W. Moore, and Z. Liang, "Fast and adaptive detection of pulmonary nodules in thoracic CT images using a hierarchical vector quantization scheme," *IEEE Journal of Biomedical and Health Informatics*, vol. 19, no. 2, pp. 648–659, 2015.

[11] A. A. A. Setio, A. Traverso, T. de Bel, M. S. N. Berens, C. van den Bogaard, P. Cerello, H. Chen, Q. Dou, M. E. Fantacci, B. Geurts, R. van der Gugten, P. A. Heng, B. Jansen, M. M. J. de Kaste, V. Kotov, J. Y.-H. Lin, J. T. M. C. Manders, A. Sóñora-Mengana, J. C. García-Naranjo, E. Papavasileiou, M. Prokop, M. Saletta, C. M. Schaefer-Prokop, E. T. Scholten, L. Scholten, M. M. Snoeren, E. L. Torres, J. Vandemeulebroucke, N. Walasek, G. C. A. Zuidhof, B. van Ginneken, and C. Jacobs, "Validation, comparison, and combination of algorithms for automatic detection of pulmonary nodules in computed tomography images: The LUNA16 challenge," *Medical Image Analysis*, vol. 42, pp. 1–13, 2017.

[12] M. Tan, R. Deklerck, B. Jansen, M. Bister, and J. Cornelis, "A novel computer-aided lung nodule detection system for CT images," *Medical Physics*, vol. 38, no. 10, pp. 5630–5645, 2011.

[13] B. van Ginneken, A. A. A. Setio, C. Jacobs, and F. Ciompi, "Off-the-shelf convolutional neural network features for pulmonary nodule detection in computed tomography scans," in *IEEE International Symposium on Biomedical Imaging*, pp. 286–289, 2015.

[14] W. Shen, M. Zhou, F. Yang, D. Yu, D. Dong, C. Yang, Y. Zang, and J. Tian, "Multi-crop convolutional neural networks for lung nodule malignancy suspiciousness classification," *Pattern Recognition*, vol. 61, pp. 663–673, 2017.

[15] A. Masood, B. Sheng, P. Li, X. Hou, X. Wei, J. Qin, and D. Feng, "Computer-assisted decision support system in pulmonary cancer detection and stage classification on CT images," *Journal of Biomedical Informatics*, vol. 79, pp. 117–128, 2018.

[16] K. Krissian, G. Malandain, N. Ayache, R. Vaillant, and Y. Trousset, "Model based multiscale detection of 3D vessels," in *Workshop on Biomedical Image Analysis*, pp. 202–210, 1998.

[17] S. Ren, K. He, R. Girshick, and J. Sun, "Faster R-CNN: Towards real-time object detection with region proposal networks," in *Neural Information Processing Systems*, pp. 91–99, 2015.

[18] K. Simonyan and A. Zisserman, "Very deep convolutional networks for large-scale image recognition," *CoRR*, vol. abs/1409.1556, 2014.

[19] J. Long, E. Shelhamer, and T. Darrell, "Fully convolutional networks for semantic segmentation," in *IEEE Conference on Computer Vision and Pattern Recognition*, pp. 3431–3440, 2015.

[20] R. Girshick, "Fast R-CNN," in *IEEE International Conference on Computer Vision*, pp. 1440–1448, 2015.

[21] S. Ren, K. He, R. Girshick, and J. Sun, "Faster R-CNN: Towards real-time object detection with region proposal networks," *IEEE Transactions on Pattern Analysis and Machine Intelligence*, vol. 39, no. 6, pp. 1137–1149, 2017.

[22] J. Dai, Y. Li, K. He, and J. Sun, "R-FCN: Object detection via region-based fully convolutional networks," in *Neural Information Processing Systems*, pp. 379–387, 2016.

[23] K. He, X. Zhang, S. Ren, and J. Sun, "Deep residual learning for image recognition," in *IEEE Conference on Computer Vision and Pattern Recognition*, pp. 770–778, 2016.

[24] S. G. Armato III, G. McLennan, L. Bidaut, M. F. McNitt-Gray, C. R. Meyer, A. P. Reeves, B. Zhao, D. R. Aberle, C. I. Henschke, E. A. Hoffman, E. A. Kazerooni, H. MacMahon, E. J. R. van Beek, D. Yankelevitz, A. M. Biancardi, P. H. Bland, M. S. Brown, R. M. Engelmann, G. E. Laderach, D. Max, R. C. Pais, D. P.-Y. Qing, R. Y. Roberts, A. R. Smith, A. Starkey, P. Batra, P. Caligiuri, A. Farooqi, G. W. Gladish, C. M. Jude, R. F. Munden, I. Petkovska, L. E. Quint, L. H. Schwartz, B. Sundaram, L. E. Dodd, C. Fenimore, D. Gur, N. Petrick, J. Freymann, J. Kirby, B. Hughes, A. Vande Casteele, S. Gupte, M. Sallam, M. D. Heath, M. H. Kuhn, E. Dharaiya, R. Burns, D. S. Fryd, M. Salganicoff, V. Anand, U. Shreter, S. Vastagh, B. Y. Croft, and L. P. Clarke, "The lung image database consortium (LIDC) and image database resource

TABLE VII: Comparison of Proposed mRFCN with existing methods on CT-Scans dataset using different performance evaluation metrics namely Sensitivity, Standard Deviation Detection Error Rate (Std $e_{D,C}$), FP per section, FP per case, ANODE Score and Processing-time (minutes).

Study	Method	Feature Set	No. of Nodules	Sensitivity	Std Std $e_{D,C}$	FPs per Section	FPs per Case	mANODE Score	Time (min)
Armato III et al. 1999 [4]	LDA & Rule Based	9	171	70 %	4.22±0.27	3	42.2	0.543	-
Gurcan et al. 2002 [26]	Rule Based & LDA	6	63	84 %	1.45±0.761	5.48	1.74	0.53	-
Armato III et al. 2002 [27]	Cascade Classifier	9	50	80%	1.24±0.51	1.0	28	0.558	-
Brown et al. 2005 [28]	Fuzzy Matching	4	36	86.4 %	1.55±0.44	11	1.44	0.564	-
Narayanan et al. 2016 [29]	Quadratic, Linear, FLD	300	112	62.27%	1.61±0.99	6.89	7.05	0.5604	-
Narayanan et al. 2018 [30]	SVM	503	1141	82.82 %	1.79±0.64	8.11	7.80	0.71	-
Jaeger et al. 2018 [31]	FPN & Retina U-Net	64	1319	73.9 %	1.79±0.95	2.82	4.2	0.629	5-6
Narayanan et al. 2018 [32]	SFS	39	192	92.38%	1.7± 0.6	7.75	7.37	0.597	-
Narayanan et al. 2019 [33]	Cluster-Based & SFS	300	280	87.86 %	1.97±0.90	5	3.0	0.749	-
Masood et al. 2020 [34]	mRPN & 3DDCNN	-	2361	98.4%	1.4±2.48	1.97	4.34	0.713	3.6-4.2
mRFCN	mLRPN & PSSM	-	892	98.1%	1.4±2.48	2.4	5.10	0.697	3.6-4.2

initiative (IDRI): A completed reference database of lung nodules on CT scans," *Medical Physics*, vol. 38, no. 2, pp. 915–931, 2011.

[25] Y. Tsuchiya, Y. Kodera, R. Tanaka, and S. Sanada, "Quantitative kinetic analysis of lung nodules using the temporal subtraction technique in dynamic chest radiographies performed with a flat panel detector," *Journal of Digital Imaging*, vol. 22, no. 2, pp. 126–135, 2009.

[26] M. N. Gurcan, B. Sahiner, N. Petrick, H.-P. Chan, E. A. Kazerooni, P. N. Cascade, and L. Hadjiiski, "Lung nodule detection on thoracic computed tomography images: Preliminary evaluation of a computer-aided diagnosis system," *Medical Physics*, vol. 29, no. 11, pp. 2552–2558, 2002.

[27] S. G. Armato III, F. Li, M. L. Giger, H. MacMahon, S. Sone, and K. Doi, "Lung cancer: Performance of automated lung nodule detection applied to cancers missed in a CT screening program," *Radiology*, vol. 225, no. 3, pp. 685–692, 2002.

[28] M. S. Brown, J. G. Goldin, S. Rogers, H. J. Kim, R. D. Suh, M. F. McNitt-Gray, S. K. Shah, D. Truong, K. Brown, J. W. Sayre, D. W. Gjertson, P. Batra, and D. R. Aberle, "Computer-aided lung nodule detection in CT: Results of large-scale observer test1," *Academic Radiology*, vol. 12, no. 6, pp. 681–686, 2005.

[29] B. N. Narayanan, R. C. Hardie, and T. M. Kebede, "Analysis of various classification techniques for computer aided detection system of pulmonary nodules in CT," in *IEEE National Aerospace and Electronics Conference and Ohio Innovation Summit*, pp. 88–93, 2016.

[30] B. N. Narayanan, R. C. Hardie, and T. M. Kebede, "Performance analysis of feature selection techniques for support vector machine and its application for lung nodule detection," in *IEEE National Aerospace and Electronics Conference*, pp. 262–266, 2018.

[31] P. F. Jaeger, S. A. A. Kohl, S. Bickelhaupt, F. Isensee, T. A. Kuder, H.-P. Schlemmer, and K. H. Maier-Hein, "Retina U-Net: Embarrassingly simple exploitation of segmentation supervision for medical object detection," *CoRR*, vol. abs/1811.08661, pp. 1–10, 2018.

[32] B. N. Narayanan, R. C. Hardie, and T. M. Kebede, "Performance analysis of a computer-aided detection system for lung nodules in CT at different slice thicknesses," *Journal of Medical Imaging*, vol. 5, no. 1, pp. 014504:1–014504:10, 2018.

[33] B. N. Narayanan, R. C. Hardie, T. M. Kebede, and M. J. Sprague, "Optimized feature selection-based clustering approach for computer-aided detection of lung nodules in different modalities," *Pattern Analysis and Applications*, vol. 22, pp. 559–571, 2019.

[34] A. Masood, P. Yang, B. Sheng, H. Li, P. Li, J. Qin, V. Lanfranchi, J. Kim, and D. D. Feng, "Cloud-based automated clinical decision support system for detection and diagnosis of lung cancer in chest CT," *IEEE Journal of Translational Engineering in Health and Medicine*, vol. 8, pp. 4300113:1–4300113:13, 2020.